Korean J. Chem. Eng., 34(4), 969-976 (2017)
DOI: 10.1007/s11814-017-0004-6

pISSN: 0256-1115
eISSN: 1975-7220

Computational fluid dynamics on the hydrodynamic characteristics of the conical cap tray

Taleb Zarei*,†, Ehsan Abedini*, Rahbar Rahimi, and Jamshid Khorshidi***

*Department of Mechanical Engineering, University of Hormozgan, Bandar Abbas, Iran
**Department of Chemical Engineering, University of Sistan and Baluchestan, Zahedan, Iran
(*Received 22 September 2016 • accepted 2 January 2017*)

Abstract−This paper addresses an investigation on the hydrodynamic behavior of a new type of cap trays called conical cap tray (ConCap tray). A 3-D computational fluid dynamics model was developed to predict the hydrodynamics of the ConCap tray which is operated in the spray regime. The model considers two phase flow of gas and liquid in a VOF-like code framework. The homogeneous multiple size group model (MUSIG model) and shear stress transport (SST) turbulence model were implemented. Detailed insights into the hydrodynamic behavior of the inside of the cones were obtained. The relation between velocity, pressure and cross section area of the flow inside the cone also was formulated. The computational fluid dynamic (CFD) results show that the pressure variation in the cones forces the liquid on the tray to be highly turbulent, which leads to deform the interface to break up. Effect of different riser heights was also studied by CFD simulations. The results show that the riser height has a significant role in the hydrodynamics of the tray, especially in uniform gas distribution in the tray and reducing weeping rates.

Keywords: Conical Cap Tray, Hydrodynamic, VOF Model, Riser Height, Spray Regime

INTRODUCTION

In the last two decades, considerable efforts have been made to improve distillation tray characteristics. Some of the improvements have been made on the basis of the sieve and valve trays such as fixed valve trays [1-4], high-powered adaptive valve tray (HAVTH) [5], FGS-VT tray [6]. Some others have introduced new design of trays such as Nye trays [7], MD trays [8], Swirltube, ConSep [9-11], Ultra-Frac [12,13], CoFlo [14,15], UOP SimulFlow [16,17], JCTP-Coflow [18], chimney type centrifugal trays [19], ripple tray [20] and elliptical tray [21]. These efforts are in answer to the need for a more sustainable distillation process.

Recently, a novel cap tray, which is a new type of cap tray, called conical cap tray (ConCap tray), was introduced [22]. Tray geometry is depicted in Fig. 1. Tray details have been described in our previous article [22]. This article shows that the new tray shares some advantages with the bubble cap tray, such as good turn down ratio, while the pressure drop of the ConCap tray is smaller than that of the bubble cap tray. The pressure drop of the ConCap tray is in the range of the valve tray [22]. The weeping and entrainment rates of the tray are acceptable in comparison with bubble cap and valve trays [22].

The goal of the present work was to study the ConCap tray hydraulic behavior by using CFD tools in different operating conditions. Computational fluid dynamics was used to minimize the experimental effort and to describe and analyze the influence of various parameters inside the ConCap tray. Numerous researchers [4,23-33] have shown that CFD simulations can be a design tool for various types of distillation trays. The key to a proper simulation on the tray is a proper estimation of the momentum exchange, or drag coefficient between gas and liquid phases. Most of these simulations use a procedure proposed by Krishna [25] for predicting the drag coefficient in the Eulerian framework. The success of these CFD techniques is so far restricted to the froth regime. To describe the spray regime, more reliable models will be required. The spray regime was observed in this novel tray [22].

Most numerical simulations of bubble formation and dynamics in the liquids have been carried out by powerful volume of fluid (VOF) model based on the concept of a fractional volume of fluid to treat the complicated gas-liquid interface [34]. Hoffman et al. [35] employed the commercial CFX 5.6, ANSYS Inc. to validate a VOF-like code for two- and three-phase film flows under transient conditions where one phase was air. A Euler-Euler algorithm for multiphase calculations with free surface was used. It has been shown that a VOF-like code is capable of describing a film break up and rivulet flow. Shojaee et al. [36] used the same model to investigate the effect of gas and liquid velocities on the effective area of the Gempak 2A structured packing. Alizadehdakhel et al. [37] introduced a VOF model using commercial CFD package FLUENT 6.2 to model the gas-liquid flow in a valve tray column. The CFD results were validated by their experiments. A single valve tray in a 30 cm column diameter was simulated. The effect of valve weight has been investigated using three valves having different weights. Malvin et al. [38,39] proposed the VOF-LES model for the hydrodynamics of distillation sieve tray and compared with Gesit et al.'s [23] work. They showed that the model was highly accurate in the optimization of tray design.

The ConCap tray CFD model must be able to predict surface

†To whom correspondence should be addressed.
E-mail: talebzarei@hormozgan.ac.ir, talebzarei@gmail.com

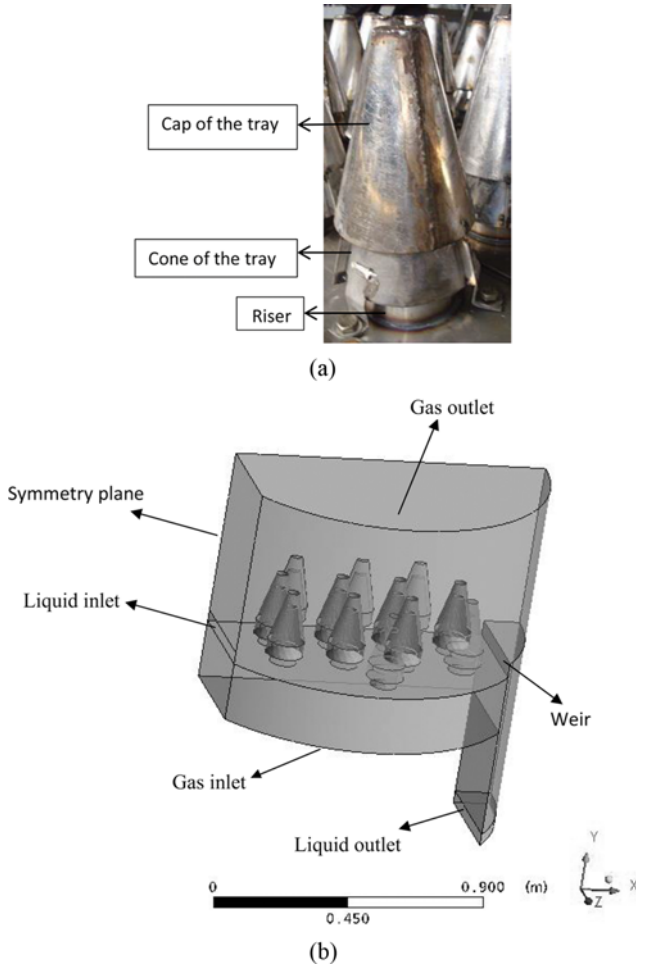

Fig. 1. (a) Photo of a cap of the ConCap tray, (b) flow geometry and boundary conditions of the ConCap tray.

breakup, droplet and rivulet formation and finally spray regime in the tray properly. In this article, by using commercial CFX code and based on the experimental work [22] a CFD model is introduced, Cto simulate ConCap tray hydrodynamics. VOF-like code method was used to simulate 1.2 m onical cap tray with 21 caps. The gas and liquid behavior inside and outside of the cones were investigated. The mechanism of bubble formation and liquid dispersion and effect of the different riser heights on the tray performance were studied.

CFD MODELING

1. Model Description

In this work, we used a Euler-Euler approach for multiphase calculations with free surfaces. CFD calculations were carried out with the commercial code CFX 11.0, ANSYS Inc. Like the VOF method [40], it uses averaged phase fractions in the finite volume cells. In case of strong interaction between the phases, it is sufficient to reduce the model to one velocity field for all phases [41]. This VOF-like code is a limiting case of Eulerian-Eulerian multiphase flow in CFX where all fluids share the same velocity fields and other relevant fields such as temperature and turbulence. Therefore, VOF-like code solves a single set of momentum equations throughout the domain, while keeping track of the volume of the phases in each computational cell. The resulting velocity in each cell is the mass-averaged value of the phases present in the cell. The corresponding momentum balance equation for the two-phase flow is given as:

$$\frac{\partial \rho \mathbf{u}}{\partial t} + \nabla \cdot (\rho \mathbf{u}\mathbf{u} - \mu(\nabla \mathbf{u} + (\nabla \mathbf{u})^T)) = S_M - \nabla p \quad (1)$$

where, S_M is the sum of the gravitational and continuum surface forces (CSF). In Eq. (1), the density (ρ) and viscosity (μ) of the fluid depend on the volume fractions of each phase and are calculated by the following equations:

$$\rho = r_1\rho_1 + r_2\rho_2 \quad (2)$$

$$\mu = r_1\mu_1 + r_2\mu_2 \quad (3)$$

In this model, the inter-phase transfer terms are all eliminated and a single phase transported equation, with variable density and viscosity is used. In this method, the surface tension force, which holds the interface together, is incorporated into the flow momentum equation as a source term using the continuum surface force (CSF) method [42].

Shear-stress-transport (SST) [43,44] is used for turbulence model which is a two-equation eddy viscosity model. This model is a combination of the k-ω model in the inner boundary layer and k-ε model on the outside of the boundary layer. The SST formulation switches to k-ε behavior in the free-stream and thereby avoids the common k-ω problem that the model is too sensitive to the inlet free-stream turbulence properties. The SST model accounts for the transport of the turbulent shear stress and gives highly accurate predictions of the onset and the amount of flow separation under adverse pressure gradients and has automatic wall treatment. The SST model was developed to overcome deficiencies in the k-ω and BSL k-ω models. The model is a good choice for most flows and is recommended for highly swirling, 3-D and rotating flows [41].

Liquid flows with poly dispersed of the liquid drops have been observed in the experiments of the ConCap tray. Therefore, the multiple size group Model (MUSIG model) implemented by CFX was used. This model solves only one common momentum equation for all bubble size classes (homogeneous MUSIG model) where the slip velocities of particles are almost independent of particle size. Liquid drops (sprays) in a gas phase can be modeled with a homogeneous MUSIG model [41]. Mathematically, the MUSIG is based on the population balance method and the two fluid modeling approaches. The dispersed phase (liquid) is divided into 5 size fractions. A range of 0 to 15 mm is used for mean drop diameter. The population balance equation is used to describe the mass conservation of the size fractions, and it accounts for the inter-fraction mass transfer caused by bubble coalescence and breakup [45]. The bubble coalescence model considers the random collision processes between two bubbles. The model is based on the work of Prince et al. [46]. The bubble breakup model considers that the collision between the liquid turbulent eddies are based on the work Luo et al. [47].

Table 1. Tray characteristic of the ConCap tray

Tray diameter, mm	1200	Riser height, mm	55
Tray spacing, mm	610	Percentage of hole area	14%
Weir length, mm	730	Active area, mm^2	1007760
Downcomer clearance, mm	40	Top Radius of the cones, mm	20
Riser diameter, mm	90	Bottom Radius of the cones, mm	63
No. of caps	21	Vertical distance between the cones, mm	50
Tray thickness, mm	2	Weir height (adjustable), mm	50

Table 2. Pressure drop at different mesh sizes

	Fine	Medium	Coarse
No. of computational nodes	134267	106379	59722
Total number of tetrahedrons	695091	559992	299973
Pressure drop (pa)	310	312	364

2. Geometric Model

Geometry and operating conditions of the model are exactly based on our experimental tests [22]. Table 1 shows characteristics of the conical cap tray. Fig. 1 shows the geometry and boundary conditions of the ConCap tray. Due to the existence of a symmetry plane for the purpose of reduction of computational effort, only half of the tray was simulated. Plane z=0 is the plane of symmetry. The actual dimension of the tray was simulated. Inlet gas flows through the chamber uniformly. This chamber with 20 cm height is located below the tray deck. It was assumed that the gas in the lower tray becomes uniform at this position. This chamber leads to better and more realistic gas distribution to the tray. Weep phenomena can be also observed in this model qualitatively.

To ensure the independence of the solution to the mesh size, the geometry was meshed using three different grid sizes. Table 2 shows the predicted pressure drop using various mesh sizes. Unstructured tetrahedral volume meshes were used in simulations due to the complexity of geometry by use of ANSYS Workbench 11.0.

3. Initial and Boundary Conditions

A good initialization guess can reduce computational time and avoid divergence. The gas and liquid that were simulated are air and water at 25 degrees Celsius and at atmospheric pressure. Initially, the water volume fraction was set to one until the weir height (5 cm) on the tray and the downcomer filled with water to the height of 0.275 m, and was set at zero in the other regions. The superficial gas velocity was used as an initial guess for the vertical component of the gas velocity throughout the computational domain, and a uniform horizontal velocity distribution that is equal to the liquid inlet velocity was specified on the tray. A parabolic liquid inlet velocity profile was introduced [23,27,28]. No-slip wall boundary condition was specified for the liquid phase and a free slip wall boundary condition was used in the gas phase. At the plane of symmetry, the normal component of velocity is zero and the gradients of the other variables in the transverse direction are taken to be zero.

RESULTS AND DISCUSSION

For the present simulation, the phases were gas (air) and liquid (water). The fluids were assumed to be Newtonian, isothermal, and incompressible; therefore, their properties were kept constant. In this section height of the weir was 5 cm and the riser was 5.5 cm. The liquid flow rate of 44.4 m^3/(mh) was used in all simulations. The calculations were under unsteady conditions, with a time step of 0.002 sec to achieve a pseudo steady state. The pseudo steady state condition was achieved after 5 seconds as depicted in Fig. 2.

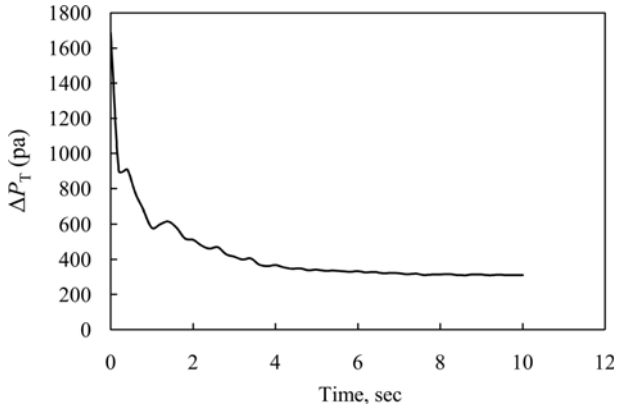

Fig. 2. Quasi steady state approach based on the total pressure drop at F_s=0.46 m/s(kg/m^3)$^{0.5}$.

Fig. 3 shows the contour of the liquid volume fraction on the tray at the F_s=0.74 m/s(kg/m^3)$^{0.5}$ and liquid flow rate of the 44.4 m^3/(mh) at different plane. According to the figure, liquid flows on the tray deck from the liquid inlet. The gas goes upward from the gas inlet in the chamber to the risers and consequently goes into the cones. As seen in the figure, the spray regime was simulated in accordance with the experimental tests. The gas was continuous phase while the liquid was the dispersed phase, which was present in the form of drops and films. A small pool of liquid or froth existed near the tray floor. As the gas passed through the cones, it drew up liquid into ligaments and tore them up into drops. The bulk of the liquid was present as drops that reside at high evaluations above the tray and follow free trajectories. Some may be entrained to the tray above, while others may fall back into the liquid pool. This flow regime is spray [48]. Therefore, the CFD model enables us to predict it (Fig. 3).

Fig. 4 shows the velocity vectors for the gas as it flows through the cones. The figure shows that as the gas leaves the gas inlet in the chamber, it hits the column tray deck wall and goes up toward the cones. When it goes toward the cone, the velocity increases and achieves the maximum value at the throat of the cone. Then, the pass way of the gas changes and goes toward between the cone

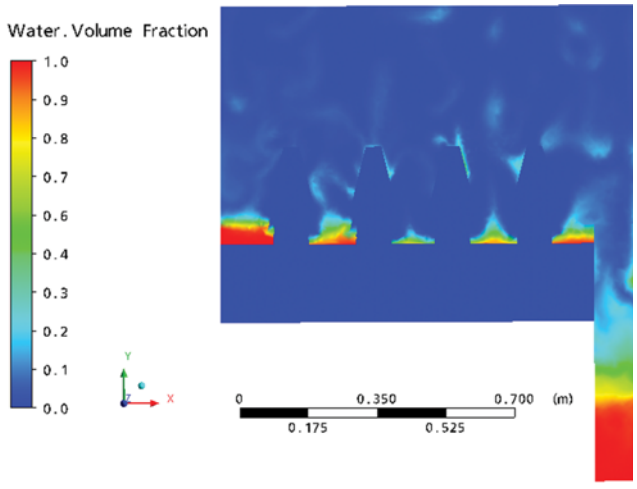

(a)

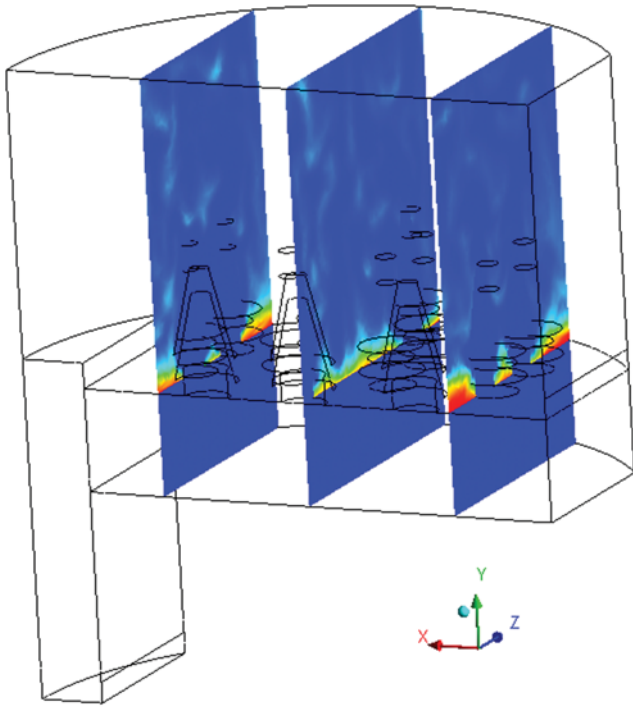

(b)

Fig. 3. Snapshots of liquid volume fraction profiles (a) on a vertical section of 0.16 m from the tray center (b) on (YZ) plane at x= 0.2. 0.5 and 0.8 m, at F_s=0.74 m/s(kg/m^3)$^{0.5}$ and t=8 sec.

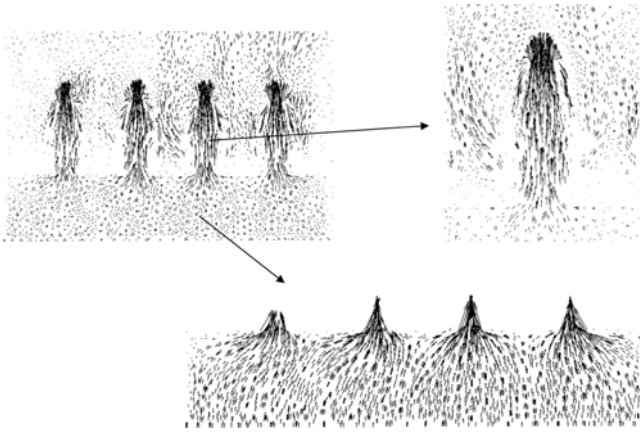

Fig. 4. Gas velocity vectors on a vertical section of 0.16 m from the tray center at F_s=0.74 m/s(kg/m^3)$^{0.5}$ and t=8 sec.

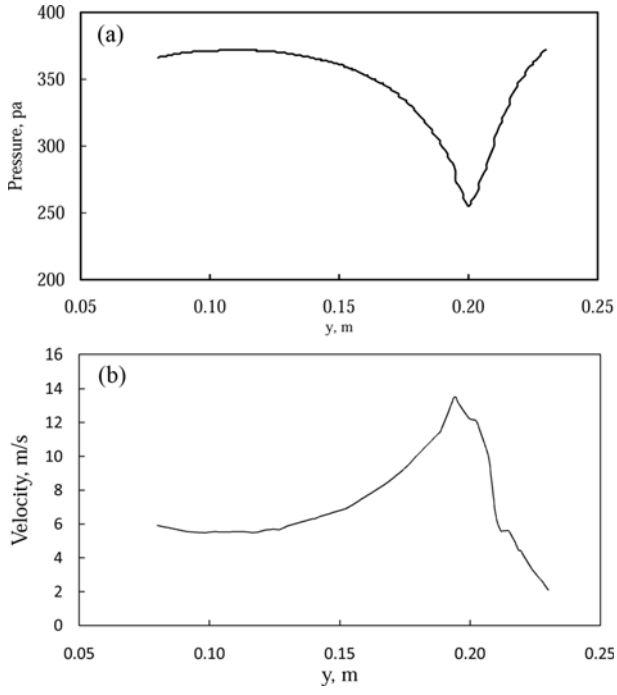

Fig. 5. (a) Total pressure drop variation along the height of cone at F_s=0.74 m/s(kg/m^3)$^{0.5}$ and t=8 sec (b) velocity variation along the height of the cone at F_s=0.74 m/s(kg/m^3)$^{0.5}$ at t=8 sec.

and cap and contact with the sprayed liquid and then moves up. The gas distribution in all the cones at this section of the plane seems uniform.

Fig. 5(a) shows the pressure variation in the cone and the space above it. The value of pressure decreases in the cone until the throat of the cone. The pressure increases in the top space between the cone and cap. The flow pattern in the cone is like subsonic flow in a nozzle. The flow in the cone, as it is seen in Fig. 5(a), is a favorable pressure gradient (i.e., dP/dy<0) and never separates, even in the throat cone where the pressure gradient is approximately zero. In a favorable gradient, the velocity profile is very rounded. There is no point of inflection. In a zero pressure gradient in the throat, the point of inflection is on the wall itself and there can be also no separation [49]. The air velocity in the cone increases until the throat of the cone and then decreases in the space between the cone and cap as it is seen in the Fig. 5(b).

The relation between velocity, pressure and cross section area of the flow inside the cone also has been formulated as follows.

From conservation of the mass:

$$\dot{m} = \rho V A = \text{constant} \tag{4}$$

If we differentiate Eq. (4):

$$VAd\rho + \rho AdV + \rho VdA = 0 \tag{5}$$

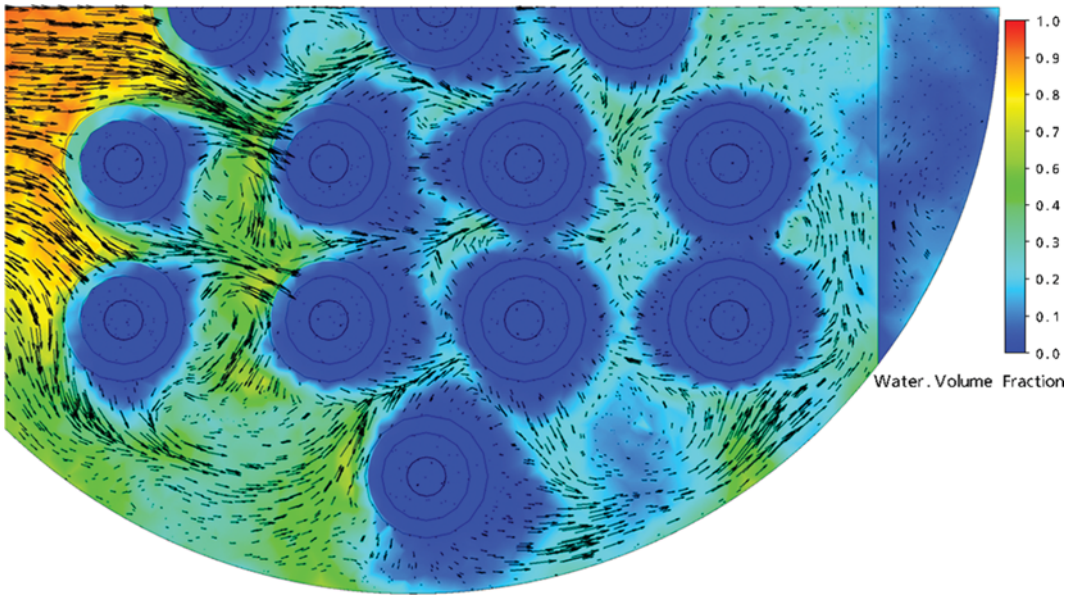

Fig. 6. Liquid volume fraction profiles and velocity vector plots on the plane at y=0.03 cm at F_s=0.74 m/s(kg/m^3)$^{0.5}$ and t=8 sec.

Then, dividing by (VAρ)

$$\frac{d\rho}{\rho}+\frac{dV}{V}+\frac{dA}{A}=0 \tag{6}$$

And from conservation of the momentum:

$$\rho V dV=-dP \tag{7}$$

For isentropic flow, we have the following equation:

$$\frac{dP}{P}=\gamma\frac{d\rho}{\rho} \tag{8}$$

Eq. (8) in combination with the equation of the state, P/ρ=RT, gives the Eq. (9) for dP:

$$dP=\gamma RTd\rho=a^2d\rho \tag{9}$$

Using a combination of Eq. (9) with momentum equation provides:

$$-M^2\frac{dV}{V}=\frac{d\rho}{\rho} \tag{10}$$

Now we substitute Eq. (10) into the mass flow equation to get:

$$(1-M^2)\frac{dV}{V}=-\frac{dA}{A} \tag{11}$$

And therefore, the relation between velocity and pressure obtains:

$$-M^2\frac{dV}{V}=\frac{1}{\gamma}\frac{dP}{P} \tag{12}$$

For subsonic flows, decrease in the cross-sectional area (dA<0) causes an increase in the flow velocity (dV>0).

The changes in the gas velocity and area sections of the cone and subsequently the change in the pressure drop cause the liquid to break up and arise or appear as sprayed droplets as shown in Fig. 3. On the other hand, the pressure variation in the cones forces the liquid on the tray to be highly turbulent. A sufficient level of turbulence in the liquid phase will deform the interface and lead to break up. More precisely, if a turbulent eddy has sufficient energy it may defeat the stabilizing effect of surface tension [50].

Fig. 6 shows water volume fraction contour and liquid velocity vectors at 3 cm above the tray deck. Nonuniform liquid velocity pattern, turbulence and circulating motion and liquid flow separation in the behind of the risers were observed. As mentioned, the SST turbulence model can simulate the separation flows. The liquid velocity decreases in the space between the cones in the exit half of the tray. Swirl and back flow movement occurred due to the gas effect and cone arrangement on the liquid flow. Each cone affects the liquid flow when the gas goes up in the cones. The liquid is thrown around because of the pressure gradient in the cones. In this level of the tray the liquid phase converts to the droplets and gets dispersed.

1. Comparison of the CFD Predictions and Experimental Results

The experimental conditions for the ConCap tray were used in the

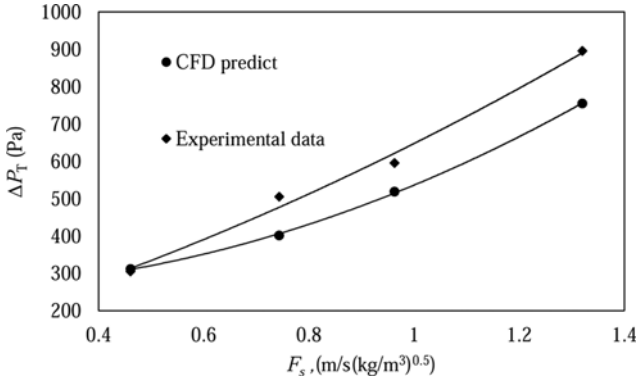

Fig. 7. Total pressure drop of the ConCap tray at the liquid flow rate of 44.4 m^3/(mh).

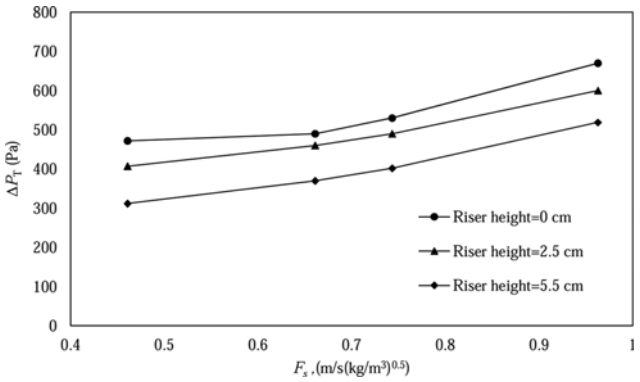

Fig. 8. Total pressure drop of the ConCap tray at different riser heights and at the liquid flow rate of 44.4 m^3/(mh).

computational model and the corresponding flow properties were evaluated. Fig. 7 shows the simulated pressure drop for two-phase air-water flow when transient simulations are time averaged, which was compared with experimental results [22]. The average error between computational and experimental results was 13.5%. Here, a liquid velocity of 44.4 m^3/(mh) and different F-factors were used.

2. Effect of the Riser Height on the Pressure Drop of the ConCap Tray

The pressure drops of the ConCap tray were studied computationally at different riser heights (0, 2.5, 5.5 cm). Fig. 8 illustrates the effect of the riser height on the total pressure drop in the liquid flow rate of 44.4 m^3/(mh). The total pressure drop increases when the riser height is decreased.

As seen in the Fig. 9, a heavy weeping rate occurred in the riser heights of zero and 2.5 cm at F_s=0.46 m/s(kg/m^3)$^{0.5}$. The weeping rate of the riser height of zero is more than a riser height of 2.5 cm and it happens mostly in the earlier cones near to the liquid inlet.

The gas velocity vectors of the tray without riser are shown in Fig. 10. In this section, there are four cones. Because of the heavy weeping in the riser heights of zero and 2.5 cm (Fig. 9), the gas cannot enter earlier cones (see cone 1 in Fig. 10) and is forced to pass through other cones. The liquid blocks the pathway of the gas and forces the gas to pass from the fewer number of cones at the exit half of the tray (channeling), and this causes to increase the pressure drop of the tray with lower riser height (Fig. 9). The gas circulation motion is also observed in the chamber for lower riser height.

In Figs. 4 and 10, the riser height leads to distribute the gas in

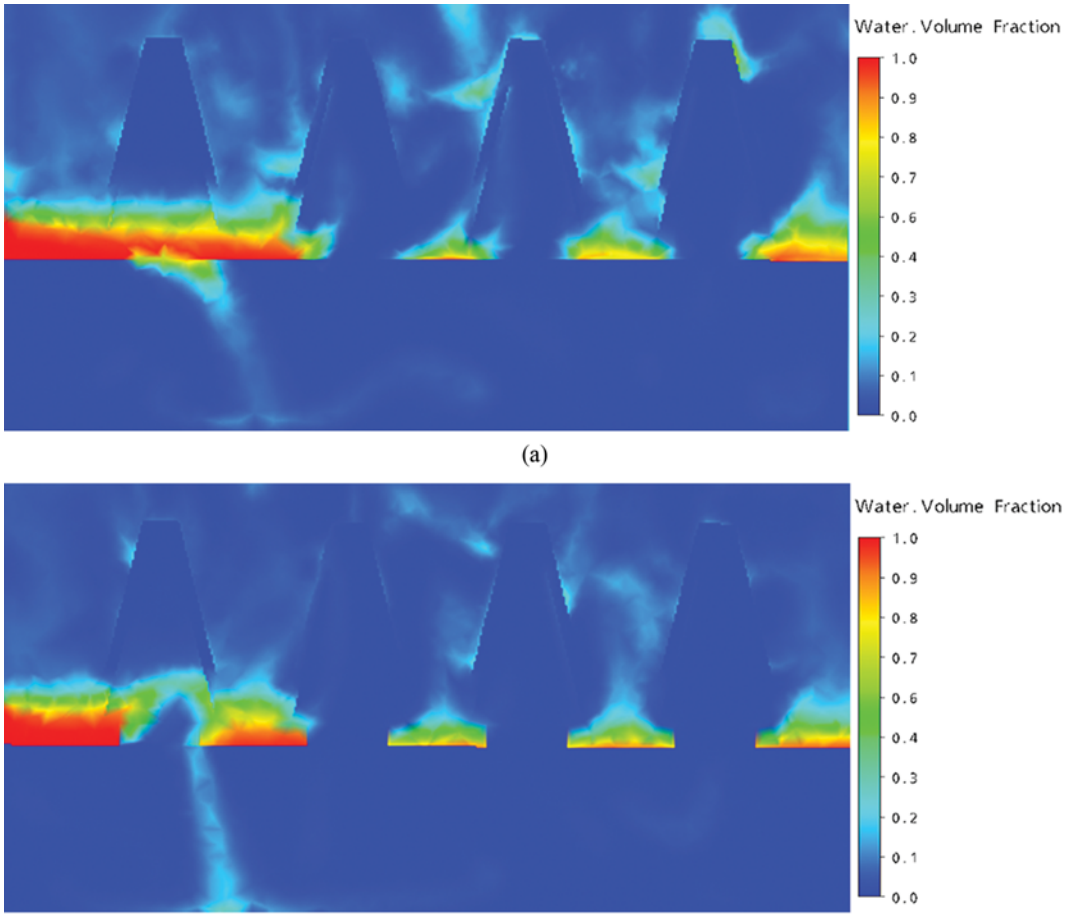

Fig. 9. Snapshots of liquid volume fraction profiles on a vertical section of 0.16 m from the center of the ConCap tray at F_s=0.46 m/s(kg/m^3)$^{0.5}$ and liquid rate of 44.4 m^3/(mh) and t=8 sec, (a) without riser height, (b) riser height of 2.5 cm.

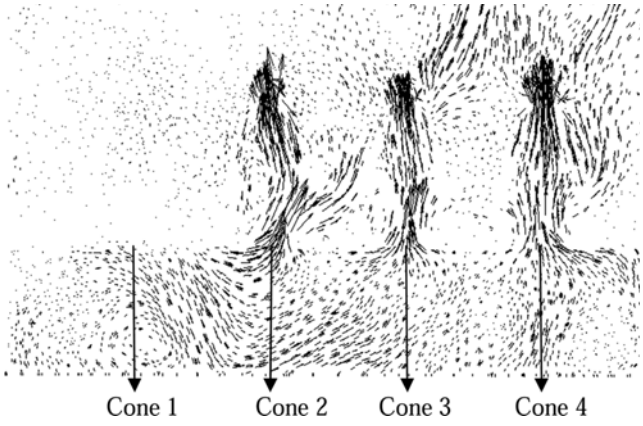

Fig. 10. Gas velocity vectors on a vertical section of 0.16 m from the tray center for the tray with riser height of zero at F_s=0.46 m/s(kg/m^3)$^{0.5}$ and t=8 sec.

the tray uniformly and prevents weeping. Nonuniform gas distribution causes to increase the pressure drop and consequently non-uniformity in the pressure gradient in the gas stream flows through the cones. Hence, the performance of the tray is reduced [48,51]. The lower riser height also leads to direct a part of the gas into the tray without entering to the cones, as seen in Fig. 10. The same behavior is observed at higher gas rates with less intensity. The weeping decreases, but the liquid on the earlier cones accumulates in the riser holes and does not permit the gas to pass through them, and channeling was also happening.

CONCLUSION

The ConCap tray is a new cap tray, so good knowledge about this novel type of tray is necessary. A numerical study was carried out in this work. The experimental column [22] was simulated in full 3D framework using VOF like code with multiple size group model and shear stress transport (SST) turbulence model. The CFD results showed a good compatibility with experimental data in terms of pressure drop. The results show the pressure variation in the cones leads to turbulence of the liquid phase and consequently deforms the interface and leads to disperse the liquid. The riser height causes the gas to distribute in the tray uniformly and prevents from weeping. The recommended riser height for the ConCap tray can be 5.5 cm because the riser diameter is very large (9 cm) in this designed tray. Lower riser height increases pressure drop and non-uniformity in the gas distributions and consequently decreases the performance of the tray. Riser height has a profound effect on the weeping of the ConCap tray. Finally, the simulation results showed that CFD can be used as an effective tool to provide information on the details of the gas and liquid flows in the tray. Further studies on the various geometries of the ConCap tray, for example, to combine it with centrifugal structure, are essential and remain for future work.

NOMENCLATURE

A : cross section of the cone [m^2]
A_T : total hole area [m^2]
a : speed of sound
F_s : F-factor=$V_S\sqrt{\rho_G}$, [m/s(kg/m^3)$^{0.5}$]
g : acceleration due to gravity [m/s^2]
M : mach number, ratio of speed of gas in the cone and the speed of sound
$\dot{m}$: mass flow rate [kg/s]
Q_L : liquid flow rate across tray, liquid flow rate per weir length [(m^3/h)/m]
R : gas constant [8.31 J/(mol K)]
r : volume fraction
T : temperature [K]
t : time [sec]
V_S : superficial gas velocity [m/s]
W : weir height [cm]
ΔP_T : tray pressure drop [Pa]
r_1 : gas volume fraction
r_2 : liquid volume fraction
S_M : sum of the gravitational and continuum surface forces
ρ_G : gas density [kg/m^3]
ρ_L : liquid density [kg/m^3]
γ : specific heat ratio, the ratio of the heat capacity at constant pressure to heat capacity at constant volume
μ : viscosity [Pa·s]

REFERENCES

1. E. Nutter, US Patent, US005360583A (1994).
2. D. E. Nutter, *Chem. Eng. Res. Des.*, **77**, 493 (1999).
3. J. Sun, X. Luo, S. Jiang, W. Wang, H. Lyu, P. Wang and H. Gao, *Chem. Eng. Technol.*, **37**, 383 (2014).
4. T. Zarei, R. Rahimi and M. Zivdar, *Korean J. Chem. Eng.*, **26**, 1213 (2009).
5. J. Qian, R. Qi and S. Zhu, *Chem. Eng. Res. Des.*, **84**, 155 (2006).
6. Q. Li, M. Zhang, X. Tang, L. Li and Z. Lei, *Chem. Eng. Res. Des.*, **91**, 970 (2013).
7. G. De Bruyn, H. A. Gangriwala and J. O. Nye, *Institution of Chemical Engineers Symposium Series 1*, (128), A509-A517 (1992).
8. J. G. Kunesh, H. Z. Kister, M. J. Lockett and J. R. Fair, *Chem. Eng. Prog.*, **91**, 43 (1995).
9. J. L. Bravo and K. A. Kusters, *Chem. Eng. Prog.*, **96**(12), 33 (2000).
10. N. Burcher, E. Wikstrom, G. Mosca, A. Hausman and P. Wilkinson, Proceedings of Topical Distillation Conference, AIChE, 189 (2007).
11. D. R. Summers, A. Bernard and W. E. D. Villiers, AIChE Proceedings of Topical Distillation Conference, 189 (2007).
12. J. Penciak, I. Nieuwoudt and G. Spencer, *IChemE Symp.*, **152**, 311 (2006).
13. P. Wilkinson, E. Vos, G. Konijn, H. Kooijman, G. Mosca and L. Tonon, *Chem. Eng. Res. Des.*, **85**, 130 (2007).
14. J. R. Fair, W. R. Trutna and A. F. Seibert, *Chem. Eng. Res. Des.*, **77**, 619 (1999).
15. W. R. Trutna, US Patent, 5,695,548 (1997).
16. Z. P. Xu and D. H. Bielinski, US Patent, 6682633B1 (2004).
17. P. Xu, B. Nowak and K. Richardson, AIChE Meeting, Spring (2007).
18. Ž. Olujić, M. Jödecke, A. Shilkin, G. Schuch and B. Kaibel, *Chem.*

Eng. Process., **48**, 1089 (2009).
19. N. Naziri, R. Zadghaffari and H. Naziri, *APCBEE Procedia*, **3**, 182 (2012).
20. N. Yang, R. Zhang, B. Jiang, Z. Li, L. Zhang and Y. Sun, *J. Taiwan Inst. Chem. Eng.*, **53**, 6 (2015).
21. X. Li, H. Cong, X. Gao and H. Li, *J. Taiwan Inst. Chem. Eng.*, **60**, 44 (2016).
22. T. Zarei, R. Rahimi, A. Zarei and M. Zivdar, *Chem. Eng. Process.*, **64**, 17 (2013).
23. G. Gesit, K. Nandakumar and K. T. Chuang, *AIChE J.*, **49**, 910 (2003).
24. S. Jiang, H. Gao, J. Sun, Y. Wang and L. Zhang, *Chem. Eng. Process.*, **52**, 74 (2012).
25. R. Krishna, J. M. Van Baten, J. Ellenberger, A. P. Higler and R. Taylor, *Chem. Eng. Res. Des.*, **77**, 639 (1999).
26. R. Rahimi, A. Zarei, T. Zarei, H. Naziri Firoozsalari and M. Zivdar, *In: 50th Distillation & Absorption Conference*, 479 (2010).
27. M. R. Ostadzehi, R. Rahimi, T. Zarei and M. Zivdar, *J. Chem. Peroluem Enineering (JCHPE)*, **47**, 39 (2013).
28. A. Zarei, R. Rahimi, T. Zarei and N. Naziri, *In: 50th Distillation & Absorption Conference*, 407 (2010).
29. S. Roshdi, N. Kasiri, S. H. Hashemabadi and J. Ivakpour, *Korean J. Chem. Eng.*, **30**, 563 (2013).
30. X. G. Li, D. X. Liu, S. M. Xu and H. Li, *Chem. Eng. Process.*, **48**, 145 (2009).
31. T. Zarei, M. Farsiani and J. Khorshidi, *Korean J. Chem. Eng.*, **34**, 150 (2017).
32. A. Zarei, S. H. Hosseini and R. Rahimi, *Chem. Eng. Res. Des.*, **91**(12), 2333 (2013).
33. A. Zarei, S. H. Hosseini and R. Rahimi, *J. Taiwan Inst. Chem. Eng.*, **44**, 27 (2013).
34. D. Ma, M. Liu, Y. Zu and C. Tang, *Chem. Eng. Sci.*, **72**, 61 (2012).
35. A. Hoffmann, I. Ausner, J.-U. Repke and G. Wozny, *Comput. Chem. Eng.*, **29**(6), 1433 (2005).
36. S. Shojaee, S. H. Hosseini, A. Rafati and G. Ahmadi, *Ind. Eng. Chem. Res.*, **5**, 10833 (2011).
37. A. Alizadehdakhel, M. Rahimi and A. A. Alsairafi, *Comput. Chem. Eng.*, **34**(1), 1 (2010).
38. A. Malvin, A. Chan and P. L. Lau, *Eng. Lett.*, **19**(1), 24 (2011).
39. A. Malvin, A. Chan and P. L. Lau, *J. Taiwan Inst. Chem. Eng.*, **45**, 1354 (2014).
40. C. W. Hirt and B. D. Nichols, *J. Comput. Phys.*, **39**, 201 (1981).
41. J. Khorshidi, T. Zarei and H. Davari, *Int. J. Industrial Mathematics*, **9**, 83 (2017).
42. J. U. Brackbill, D. B. Kothe and C. Zemach, *J. Comput. Phys.*, **100**, 335 (1992).
43. F. R. Menter, *AIAA J.*, **32**, 1598 (1994).
44. F. R. Menter and Y. Egorov, IUTAM Symposium on One Hundred Years of Boundary Layer Research, Springer, Netherlands, 279 (2006).
45. E. Krepper, M. Beyer, T. Frank, D. Lucas and H. M. Prasser, *Nucl. Eng. Des.*, **239**(11), 2372 (2009).
46. M. J. Prince and H. W. Blanch, *AIChE J.*, **36**, 1485 (1990).
47. H. Luo and H. F. Svendsen, *AIChE J.*, **42**, 1225 (1996).
48. H. Z. Kister, McGraw Hill (1992).
49. F. M. White, Fluid Mechanics, McGraw Hill (2011).
50. D. Fuster, A. Bagué, T. Boeck, L. Le Moyne, A. Leboissetier, S. Popinet, P. Ray, R. Scardovelli and S. Zaleski, *Int. J. Multiphase Flow*, **35**, 550 (2009).
51. M. J. Lockett, Cambridge University Press: Cambridge, U.K. (1986).